Local and global electrochemical impedances applied to the corrosion behaviour of an AZ91 magnesium alloy

Gonzalo Galicia [a], Nadine Pébère [b], Bernard Tribollet [a], Vincent Vivier [a,*]

[a] LISE – UPR 15 du CNRS, Université Pierre et Marie Curie, 4 place Jussieu, 75252 Paris Cedex 05, France
[b] Université de Toulouse, CIRIMAT, UPS/INPT/CNRS, ENSIACET, 118 route de Narbonne, 31077 Toulouse Cedex 04, France

A B S T R A C T

The electrochemical behaviour of an AZ91 magnesium alloy was investigated in a low aggressive medium by means of local and global electrochemical impedance measurements. The results were compared to those obtained on a pure magnesium sample. It was possible to show the individual contribution of each phase constituting the alloy, and it was observed that the corrosion mechanism of the two phases was the same, controlled by the Mg dissolution. However, local impedance diagrams clearly indicated that the kinetics dissolution of the β-phase was slower than that of the α-phase, which was in good agreement with SEM observations.

Keywords:
A. Alloy
A. Magnesium
B. EIS

1. Introduction

Electrochemical techniques such as cyclic voltammetry and electrochemical impedance spectroscopy are widely used for investigating corrosion processes [1]. From the measurements of potential and current, the kinetics of the reactions occurring on the metal surface can be determined [1,2]. However, the measured quantities (E, I) account for averaged values over the whole electrode surface, showing that the conventional electrochemical methods have major limitations for the study of heterogeneous electrochemical processes such as localized corrosion [3,4]. Since the early 1980s, a great effort has been paid for the development of spatially resolved electrochemical techniques mainly due to both the improvement of the electronic devices and the significant progress in the fabrication of the metal microelectrodes [5,6]. Today, local electrochemical techniques afford new ways to investigate localized processes and has lead to significant advances in the measurement of both heterogeneous and homogeneous reactions [7–13].

During the last decades, magnesium and magnesium alloys have received significant attention due to their increasing use as lightweight materials for various applications specially in automobile and aerospace industries [14–16]. However, magnesium exhibits a poor corrosion resistance that is exacerbated by the presence of impurities (Fe, Ni, Cu, ...) acting as local cathodes and enhancing localized corrosion processes. In addition, the anodic dissolution of Mg exhibits an unexpected behaviour due to the negative difference effect (NDE) corresponding to an increase of hydrogen production while increasing the potential [14,15]. Recently, from an impedance investigation, a corrosion mechanism was proposed to describe the behaviour of pure Mg in a sodium sulphate solution [15]. Magnesium corrosion is controlled by the presence of a very thin MgO oxide film, and dissolution occurs only at the bare parts of this film. Both the MgO and the film-free areas are covered by a thick porous layer of $Mg(OH)_2$. On the bare surface areas, the exchange of two electrons occurs in two successive electrochemical steps where the adsorption of the intermediate $(Mg^+)_{ads}$ is followed by two parallel paths; one is chemical and gives rise to the NDE and the other is electrochemical leading to Mg^{2+}. This model will be detailed in Section 4.

In the case of AZ-type magnesium alloys, their corrosion resistance was described to be strongly dependent on both the Mg content and the microstructure [17]. For instance, Nisancioglu et al. [18] have reported that the β-phase increases the corrosion resistance, whereas Das and Davis [19] have shown an increase of the corrosion (*i.e.* the dissolution of the α-phase) due to a galvanic coupling between the two phases. Mathieu et al. [20] have measured the corrosion potential of the β-phase which is 150 mV nobler than the α-phase, but the corrosion rate of the two phases were found to be similar. Song et al. [21,22] have concluded that both effects can be observed depending on the size of the β-phase, but the influence of the microstructure on the corrosion behaviour of Mg alloys still remains controversial. In recent papers, Pebere et al. [16,23] have shown that, at the corrosion potential and for short immersion times, the impedance spectra of AZ91 and AM50 magnesium alloys were similar to that obtained for pure magnesium in the same media [15]. This result, in good agreement with other literature

Corresponding author. Tel.: +33 1 4427 4158; fax: +33 1 4427 4074.
E-mail address: vincent.vivier@upmc.fr (V. Vivier).

data, indicated that the dissolution of Mg is a key parameter on the corrosion process of Mg alloys.

In a previous paper, the corrosion behaviour of an as cast AZ91 magnesium alloy has been investigated using local electrochemical impedance spectroscopy (LEIS) [24]. The LEIS experiments performed above a pit were analyzed considering that the impedance of the passive area short-circuited the impedance of the pit [4], and an electrical equivalent circuit was then devised that accounts for the obtained results. Nevertheless, the size of the probe used (in the mm range) did not allow a suitable resolution to be achieved. The scanning vibrating electrode technique (SVET) was also implemented by Williams and McMurray [25] in order to study the pit formation on pure magnesium. In that case the size of the pits mapped with this technique were larger than 1 mm, whereas optical observations clearly shown smaller-size active area on which bubbles evolved (cathodic hydrogen evolution) surrounded by an anodic ring domain corresponding to active Mg dissolution.

The present work reports a study on the electrochemical behaviour of an AZ91 magnesium alloy to determine its local reactivity by using LEIS. A special attention was paid to investigate the contributions of each phase constituting the alloy by using a probe allowing a spatial resolution in accordance with the dimension of the alloy microstructure. For comparison, the same experiments were performed on pure magnesium. Conventional electrochemical impedance spectroscopy (EIS) was also carried out on the pure Mg and on the AZ91 Mg alloy to discuss difference between global and local diagrams.

2. Experimental

2.1. Chemicals and samples

The specimen was cut from a 20 cm in diameter AZ91-alloy rod obtained by a die casting process to form a 1 cm in diameter bar. The bar was laterally insulated with a cataphoretic paint and was then embedded in an epoxy resin, forming a disk electrode of 0.79 cm^2 surface area. Prior to any experiment, the electrode was abraded with SiC paper down to grade 2400, and ultrasonically rinsed with distilled water.

A pure Mg rod (99.9+%) of 0.79 cm in diameter was purchased from Goodfellow and mounted as a disk electrode following the same procedure than for the AZ91 alloy.

The electrolyte consisted of a 1 mM Na_2SO_4 (analytical grade) solution, in contact with air, quiescent and at room temperature.

2.2. Instrumentation

The LEIS apparatus sketched in Fig. 1 was a home-made device. It consisted of a 3-axis positioning system (UTM25, Newport) mounted on an anti-vibration structure and driven by a motion encoder (MM4005, Newport) allowing a spatial resolution of 0.2 μm in the three directions. The potentials were controlled by a home-made potentiostat. The experimental setup was computer controlled by a single software developed under Labview© environment. A four-channel frequency response analyzer (Solartron – FRA 1254), allowing both global and local impedances to be recorded simultaneously was used. A low-noise analog differential amplifier with both variable gain and high input impedance was developed for recording the local potentials and current variations.

A classical three-electrode cell was used for performing global impedance measurements, whereas a dual probe (bi-electrode) was added in solution as a two-reference-electrode system for performing local impedance measurements (five-electrode configuration). The bi-electrode consisted of either two platinum wires (20 μm in diameter) or two silver wires (40 μm in diameter). The use of platinum dual-probe needs a deposit of Pt black from hydrogen hexachloroplatinate (IV) on each microdisk to reduce the interfacial impedance of these electrodes [26]. AgCl deposits were daily performed on each silver wire in order to have a dual-microreference electrode system. For both global and local impedance measurements, the working electrode was mounted face-up in a Plexiglas cell, the counter electrode was a large platinum grid surrounding the entire cell and potentials were measured with respect to a saturated calomel electrode (SCE). For data interpretations, it was assumed that the angle defined by the line of the two centres of the bi-electrode and the surface of the sample was 90°; in other words, the local contribution measured with this setup was the normal current component, only.

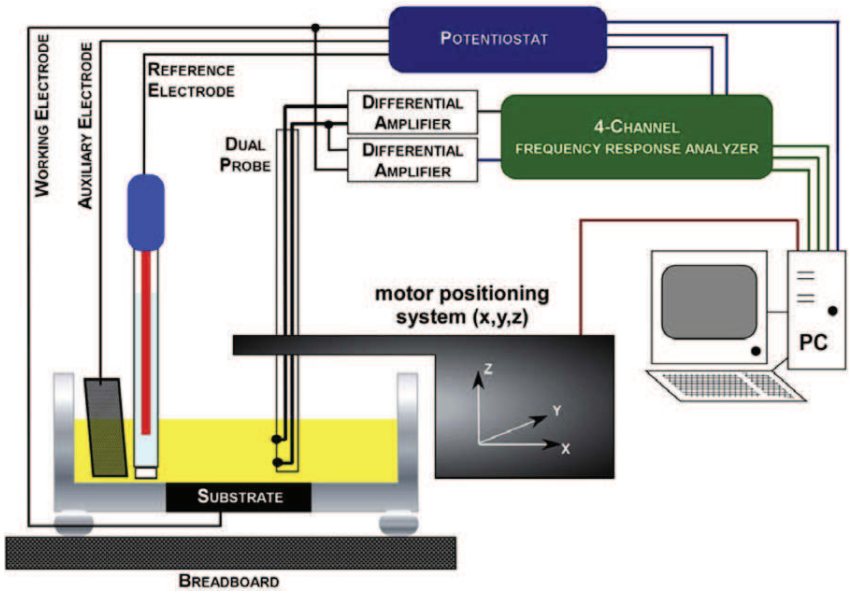

Fig. 1. Sketch of the LEIS experimental setup.

Scanning electron microscopy (SEM) observations were performed with a Leica Stereoscan 440 microscope coupled with EDS elemental semi-quantitative analyzer (Princeton Gamma-Tech) at 20 keV.

2.3. LEIS technique

The LEIS technique is based on the pioneering work of Isaacs et al. [27,28], and takes into account the recent developments of our group about the definition of the various local impedances [29–31]. Using a bi-electrode for probing solution potential distributions and a four-channel frequency response analyzer, both global and local impedances could be measured simultaneously [28,29]. In the following, the use of an upper-case letter signifies that Z is a global value; whereas, the use of a lower-case letter means that z is a local value, following the notation proposed by Huang et al. [29]. For local electrochemical measurements, the local ac-current density $i_{loc}(\omega)$ was obtained through the Ohm's law using

$$i_{loc}(\omega) = \frac{\Delta V_{probe}(\omega)\kappa}{d} \quad (1)$$

where κ is the electrolyte conductivity, $\Delta V_{probe}(\omega)$ is the ac-potential difference between the two probes, and d is the distance between the two probes.

The local impedance (z) involves the electrode potential measured with respect to a reference electrode located far from the electrode surface

$$z(\omega) = \frac{\tilde{V}(\omega) - \Phi_{\text{ref}}}{i_{loc}(\omega)} = \frac{\tilde{V}(\omega)}{\Delta V_{probe}(\omega)} \frac{d}{\kappa} \quad (2)$$

where $\tilde{V}(\omega) - \Phi_{\text{ref}}$ represents the ac-potential difference between the electrode surface and the reference electrode in the bulk solution.

3. Results

SEM observation (Fig. 2) and elemental analysis (Table 1) performed on various locations of the alloy surface clearly shown the presence of two phases: the α-phase (in dark) composed of 96.5% Mg and 3.05% Al (wt.%), and the β-phase (in grey) for which the Al content increases up to 27.5%. It should be mentioned that the surface composition can slightly change from one experiment to another due to both the heterogeneous composition of the bulk material and the successive steps of the abrading procedure between each set of experiments.

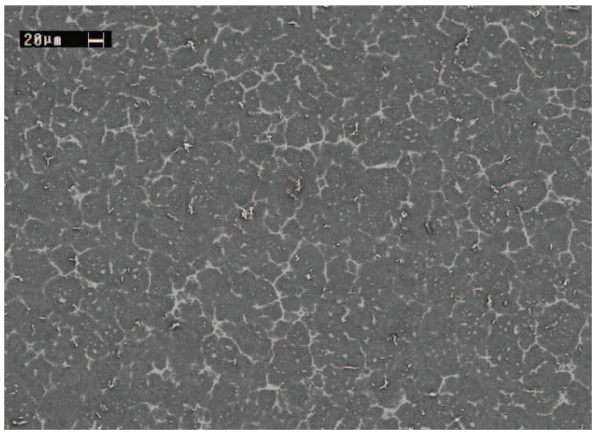

Fig. 2. SEM image of the AZ91 alloy. The dark and grey areas correspond to the α-phase and β-phase, respectively.

Table 1
Elemental composition of the AZ91 magnesium alloy (in wt.%).

Element	Mg	Al	Zn	Mn
AZ91 (mean value)	90.05	8.90	0.85	0.20
α-Phase	96.50	3.05	0.40	0.05
β-Phase	69.60	27.45	2.70	0.25

Fig. 3 shows the electrochemical impedance diagrams of pure magnesium obtained in a 1 mM Na_2SO_4 solution at the corrosion potential after 2 and 36 h of immersion. The shape of the diagrams is similar to that already obtained in more concentrated electrolytes using a rotating disk electrode [15,16]. In the high frequencies, the capacitive loop was ascribed to the charge transfer resistance; the medium-frequency time constant was attributed to diffusion processes through the corrosion products layer; and in the low frequencies, the inductive loop was ascribed to the relaxation of adsorbed species. It can be seen that the impedance increased with immersion time indicating a decrease of the corrosion rate probably due to the accumulation of corrosion products at the electrode surface. After longer immersion times (more than 5 days at the corrosion potential), impedance spectra remained unchanged with three well-defined time constants as shown in Fig. 3b. It can be noticed that the value of the electrolyte resistance is low compared to the theoretical prediction and diminishes as the time increases. This behaviour can be ascribed to the strong reactivity of the magnesium leading to the production of Mg^{2+} and OH^- in solution.

Fig. 4 shows local impedance spectra recorded with a Pt bi-microelectrode at the corrosion potential after 36 h of immersion. Position 1 corresponds to the electrode centre, whereas the probe was moved of 100 and 200 µm from the electrode centre for the positions 2 and 3, respectively. The spatial domain investi-

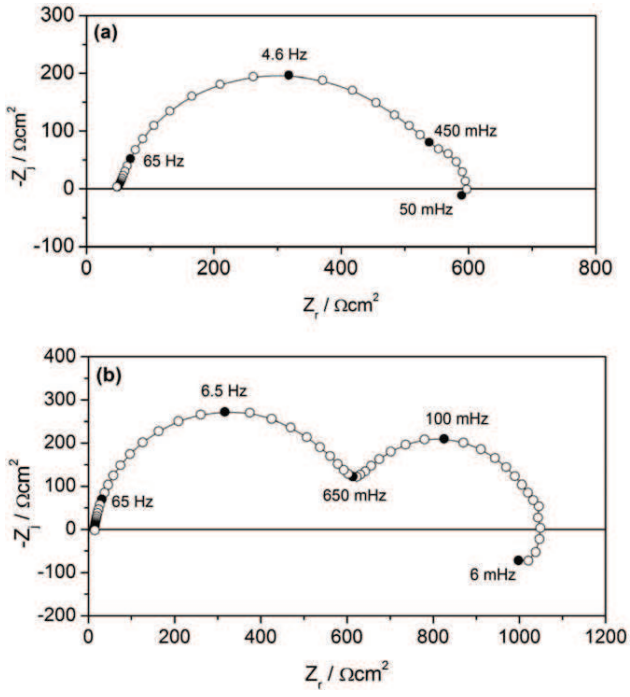

Fig. 3. Nyquist plots of the electrochemical impedance response of a pure Mg electrode in 1 mM Na_2SO_4 solution at the corrosion potential for two immersion times: 2 h (a) and 36 h (b).

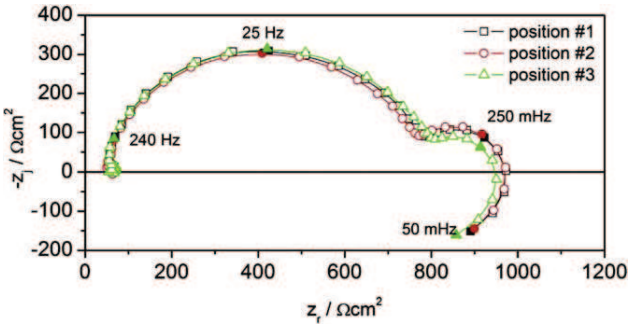

Fig. 4. Nyquist plots of the local electrochemical impedance response of a pure Mg electrode in 1 mM Na_2SO_4 solution at the corrosion potential after 36 h immersion. The spectra were recorded close to the electrode centre (see text).

gated in the present work was deliberately restricted to the electrode centre in order to minimize the radial distribution of the current density on a disk surface [29,32]. The spectra were similar and superimposable for the three positions. In the very high frequencies, LEIS spectra exhibit an inductive part. Such a behaviour is in agreement with previous observations [33,34] and must be ascribed to the cell geometry used and not to the electrochemical behaviour of the Mg sample. The other time constants easily compared with those obtained from global measurements indicating that at this time scale and with this electrolyte concentration, the Mg electrode corrodes uniformly.

The global impedance response of an AZ91 electrode in a 1 mM Na_2SO_4 solution at the corrosion potential is presented in Fig. 5 with time as parameter. The spectra show a significant evolution with time: for short immersion times (2 and 12 h), both high- and medium-frequency time constants were poorly resolved, whereas for longer immersion times (24 and 72 h), the diagrams were similar to that obtained on pure Mg.

Fig. 6 shows representative local impedance diagrams obtained with the AZ91 sample at the corrosion potential after 2 h immersion. Before starting the experiment, the dual probe was bringing into contact with the sample in order to leave a mark and to be able to locate the α- and β-phases. It was shown that the shape of the spectra was independent of the probe position. However, two main differences were always observed. Over the β-phase, the amplitude of the impedance was about three times larger than over the α-phase, and the time constant of the high frequency capacitive loop was 10 times smaller for the α-phase. This indicates that the corrosion rate of the β-phase is lower than that of the α-phase mainly due to the effect of Al as primary alloying element.

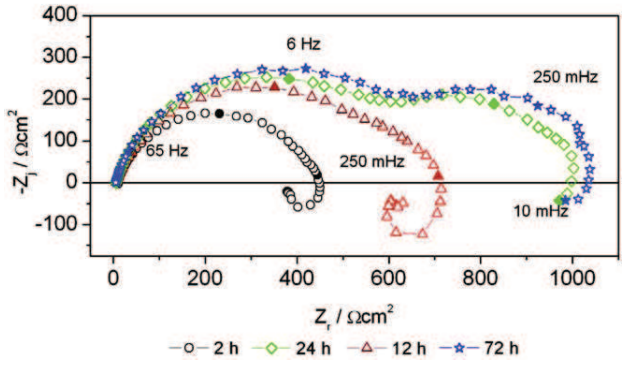

Fig. 5. Nyquist plots of the electrochemical impedance response of the AZ91 alloy in 1 mM Na_2SO_4 solution at the corrosion potential with time as parameter.

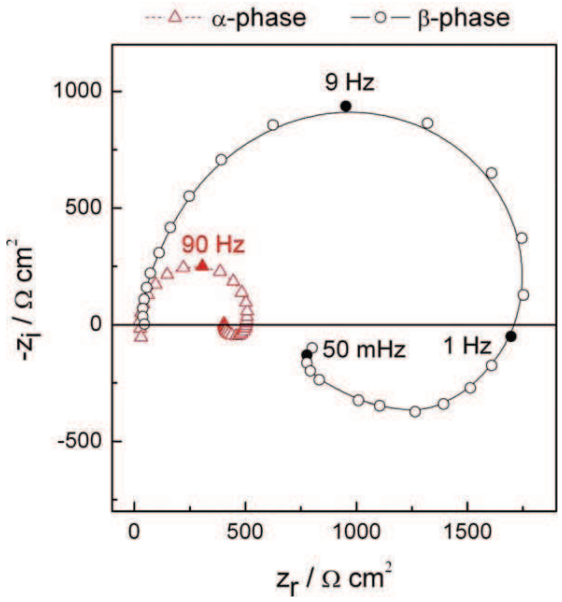

Fig. 6. Nyquist plots of the local electrochemical impedance response of the AZ91 alloy after 2 h immersion in 1 mM Na_2SO_4 solution at the corrosion potential. The spectra were recorded close to the electrode centre at various locations over the alloy.

It can be mentioned that for long immersion times, the spatial resolution of the local measurements was less accurate due to the preferential dissolution of the α-phase (higher corrosion rate) and the local impedance diagrams were not reported here.

Fig. 7 shows a SEM image of the AZ91 electrode after 24 h immersion in 1 mM Na_2SO_4 solution at the corrosion potential. The dark areas correspond to the α-phase whereas the bright domains correspond to the β-phase. It can be seen that the local reactivity of the alloys strongly depends on its local composition as previously stated. This local reactivity can also be monitored by performing a local mapping at a fixed frequency (100 Hz) and at a constant distance from the AZ91 electrode surface (Fig. 8). This mapping clearly shows the influence of Al as alloying element since the corrosion rate of the β-phase appears lower than that of the α-phase. These results concerning the reactivity of the material favourably compare with its microstructure presented in Fig. 2.

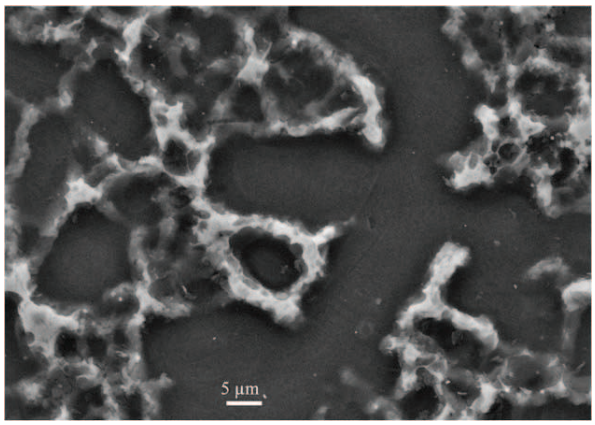

Fig. 7. SEM image of the AZ91 alloy after 24 h immersion in 1 mM Na_2SO_4 solution at the corrosion potential.

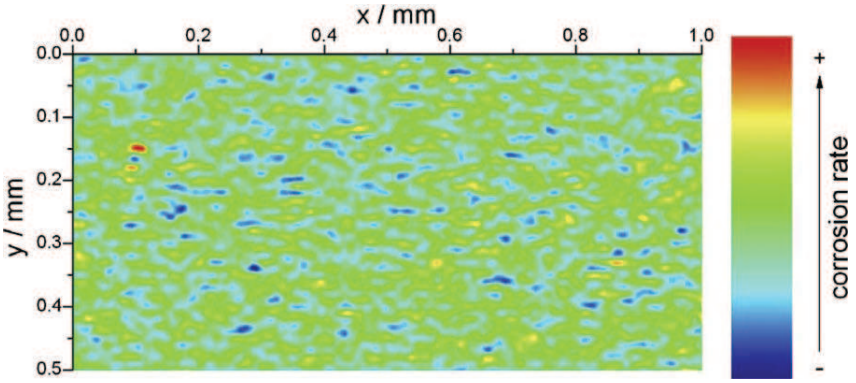

Fig. 8. LEIS image of the AZ91 alloy after 24 h immersion in 1 mM Na_2SO_4 solution at the corrosion potential. The mapping was performed at a fixed frequency (100 Hz) by moving the probe over the alloy surface.

4. Discussion

The reaction mechanism of the α-phase of the AZxx series was shown to be similar to that of a pure Mg [22]. In a recent article, Baril et al. [15] have discussed different models of the literature describing the anodic dissolution of Mg. They proposed a kinetic model that accounts for the Mg corrosion that is independent of the nature of the electrolyte. It was assumed that the Mg electrode is partially coated by a MgO thin film, the overall electrode being covered by a thick $Mg(OH)_2$ layer. On the film-free areas, the two successive electrochemical reactions considered were:

$$Mg \xrightarrow{k_1} Mg^+_{ads} + e^- \tag{3}$$

and

$$Mg^+_{ads} \underset{k_{22}}{\overset{k_2}{\rightleftharpoons}} Mg^{2+} + e^- \tag{4}$$

In the high frequencies, the capacitive loop is ascribed to the charge transfer resistance of reactions 3 and 4, in parallel to the MgO film capacitance. The second time constant in the medium frequency range corresponds to the diffusion of the Mg^{2+} ions through the porous $Mg(OH)_2$ layer. The inductive loop observed in the low frequencies is attributed to the presence of the adsorbed species Mg^+_{ads}. Finally, the NDE was described as a chemical step involving Mg^+_{ads} through:

$$Mg^+_{ads} + H_2O \xrightarrow{k_3} Mg^{2+} + OH^- + \frac{1}{2}H_2 \tag{5}$$

On the basis of these reactions, AC impedance diagrams can be calculated assuming that:

- the adsorbate Mg^+_{ads} obeys Langmuir's isotherm,
- the rate constant of electrochemical reactions obey Tafel's law,
- the thickness of the corrosion product layer is δ.

Each reaction (index i) has a normalized rate constant K_i that can be expressed as a function of its rate constant k_i by

$$K_i = k_i \exp(b_i(E - E^0)) \tag{6}$$

where b_i is the activation coefficient and E^0 is an origin potential. Assuming that the maximum number of sites per surface unit which can be occupied by the adsorbate Mg^+_{ads} is β, the mass and charge balances are expressed in Ref. [15] as functions of the fraction of the surface coverage, θ, by the adsorbed species. In Ref. [15], the authors have shown that resulting faradic impedance, Z_F, can be expressed as

$$Z_F = \frac{\Delta V}{\Delta I} = \frac{\left(1 + K_{22}N(\omega)\left(1 - \frac{(K_2\beta - K_1)}{(\beta j\omega + K_1 + \beta(K_2 + k_3))}\right)\right)}{AF\left(\frac{(r_1 - r_2)(K_2\beta - K_1)}{(\beta j\omega + K_1 + \beta(K_2 + k_3))} + (r_1 + r_2)\right)} \tag{7}$$

with $r_1 = (1 - \theta)K_1b_1$ and $r_2 = K_2b_2\beta\theta + K_{22}b_{22}C^{(0)}_{Mg^{2+}}$.

Finally, the overall impedance Z involves the contribution of the electrolyte resistance R_e, the faradic impedance Z_F, and the capacitance C_f:

$$Z = R_e + \frac{Z_F}{1 + j\omega Z_F C_f} \tag{8}$$

This reaction model allows considering various cases, and should account for the dissolution mechanism of both pure Mg and AZ91 alloy. Fig. 9 shows two simulated impedance diagrams. The black-circle curve corresponds to the same calculation performed previously for describing the Mg dissolution [15]. It is in perfect agreement with experimental results presented in this work for pure Mg (both global and local measurements) and for the longest immersion times. The red-triangle curve was obtained assuming that no diffusion occurs in the corrosion products layer.[1] This can be explained by the fact that all the Mg^{2+} ions produced at the interface react with the hydroxyl ions OH^- to give $Mg(OH)_2$ which forms the porous layer and thus the backward step of reaction 4 is negligible (K_{22} tends toward zero in Eq. (7)). In that case, the shape of the diagram was very similar to that obtained for short immersion times of both pure Mg and the AZ91 alloy. As a result, the evolution of the shape of the impedance diagrams corresponds to the formation of a corrosion products layer that thickens with time. These results also compare with those obtained by Baril et al. [23], who showed that, using a rotating disk electrode, the impedance data evolve from three well-defined time constants to a system with an apparent two well-defined time constants. In that case, one can assume that the convection pulled up the corrosion products in solution.

The dissolution model of pure magnesium appears to fit well the corrosion mechanism of the AZ91 alloy. The kinetics of the Mg dissolution is faster on the α-phase than on the β-phase. This behaviour can be ascribed to the large aluminium content of the β-phase that strongly reduces its electrochemical reactivity as shown with SEM observations (Fig. 7) and on LEIS mapping (Fig. 8). This result confirms that the corrosion behaviour of the α-phase and the β-phase in AZ magnesium alloys follows the same corrosion mechanisms as pure magnesium at least for short immersion times. However, due to the large number of parameters

[1] For interpretation of the references to color in this figure text, the reader is referred to the web version of this paper.

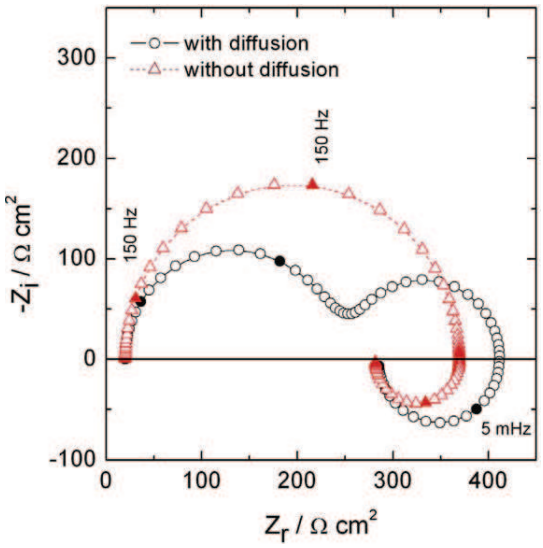

Fig. 9. Simulated impedance diagrams calculated for the following parameters: $b_1 = 20\ V^{-1}$; $b_2 = 10\ V^{-1}$; $b_{22} = 10\ V^{-1}$; $k_1 = 10^{-9}\ cm^{-2}\ s^{-1}$; $k_2 = 1.5 \times 10^{-2}\ cm^{-2}\ s^{-1}$; $k_3 = 5 \times 10^{-4}\ cm^{-2}\ s^{-1}$; $\delta = 20\ \mu m$; $D = 3 \times 10^{-6}\ cm^{-2}\ s^{-1}$; $Cdl = 20\ \mu F\ cm^{-2}$; $\beta = 1.5 \times 10^{-3}\ mol\ cm^{-2}$.

involved in the model, the results presented on this paper only account for simulations and no fitting procedure has been developed.

The analysis of the high frequencies part of the global impedance diagrams indicates a non-ideal behaviour of the electrode with a distribution of the time constant that results in a CPE (constant phase element) instead of pure capacitor. For the pure magnesium, the CPE coefficient varies from 0.75 for short immersion time to 0.82 for long immersion time, whereas it varies from 0.76 to 0.78 for the AZ91 in the same conditions. However, for both materials, the local impedance diagrams exhibited a quasi ideal behaviour in the high frequencies. The CPE behaviour observed on the global spectra was recently explained for the Mg alloy by a 2D distribution of the resistance and was not due to a capacitance dispersion as it was usually discussed [35].

5. Conclusion

LEIS experiments were performed on pure Mg and on an AZ91 alloy in low concentrated sodium sulphate solution to investigate the reactivity of the two phases of the alloy. The following points have been established:

(i) The previous model proposed for pure Mg corrosion also accounts for AZ91 corrosion.
(ii) The corrosion mechanism of the two phases constituting the AZ91 alloy was the same, controlled by the Mg dissolution, but the kinetics dissolution of the β-phase was slower than that of the α-phase.
(iii) The frequency dispersion of the high frequency capacitive loop (global impedance) was ascribed to a 2D distribution of the resistance along the electrode radius.

Acknowledgements

The authors gratefully acknowledge S. Borensztajn (UPR 15 – CNRS) for SEM and EDS analyses and D. Rose (UPR 15 – CNRS) for technical helps.

References

[1] C. Gabrielli, in: I. Rubinstein (Ed.), Physical Electrochemistry. Principles, Methods, and Applications, Marcel Dekker, New York, 1995 (Chapter 6).
[2] A.J. Bard, L.R. Faulkner, Electrochemical Methods: Fundamentals and Applications, second ed., Wiley-VCH, New York, 2001.
[3] I. Annergren, D. Thierry, F. Zou, J. Electrochem. Soc. 144 (1997) 1208–1215.
[4] R. Oltra, M. Keddam, Electrochim. Acta 35 (1990) 1619–1629.
[5] R.M. Wightman, Anal. Chem. 53 (1981) 1125A.
[6] P. Sun, F.O. Laforge, M.V. Mirkin, Phys. Chem. Chem. Phys. 9 (2007) 802–823.
[7] H.S. Isaacs, G. Kissel, J. Electrochem. Soc. 119 (1972) 1628–1632.
[8] H.S. Isaacs, M.W. Kendig, Corrosion 36 (1980) 269–274.
[9] E. Bayet, F. Huet, M. Keddam, K. Ogle, H. Takenouti, J. Electrochem. Soc. 144 (1997) L87–L90.
[10] E. Bayet, F. Huet, M. Keddam, K. Ogle, H. Takenouti, Electrochim. Acta 44 (1999) 4117–4127.
[11] C. Gabrielli, S. Joiret, M. Keddam, H. Perrot, N. Portail, P. Rousseau, V. Vivier, J. Electrochem. Soc. 153 (2006) B68–B74.
[12] A. Davoodi, J. Pan, C. Leygraf, S. Norgren, Appl. Surf. Sci. 252 (2006) 5499–5503.
[13] A. Schreiber, J.W. Schultze, M.M. Lohrengel, F. Karman, E. Kalman, Electrochim. Acta 51 (2006) 2625–2630.
[14] G.L. Song, A. Atrens, Adv. Eng. Mater. 1 (1999) 11–33.
[15] G. Baril, G. Galicia, C. Deslouis, N. Pebere, B. Tribollet, V. Vivier, J. Electrochem. Soc. 154 (2007) C108–C113.
[16] G. Baril, N. Pebere, Corros. Sci. 43 (2001) 471–484.
[17] A. Pardo, M.C. Merino, A.E. Coy, F. Viejo, R. Arrabal, S. Feliu, Electrochim. Acta 53 (2008) 7890–7902.
[18] O. Lunder, J.E. Lein, T.K. Aune, K. Nisancioglu, Corrosion 45 (1989) 741–748.
[19] S.K. Das, L.A. Davis, Mater. Sci. Eng. 98 (1988) 1–12.
[20] S. Mathieu, C. Rapin, J. Steinmetz, P. Steinmetz, Corros. Sci. 45 (2003) 2741–2755.
[21] G. Song, A. Atrens, Adv. Eng. Mater. 5 (2003) 837–858.
[22] G. Song, A. Atrens, X. Wu, B. Zhang, Corros. Sci. 40 (1998) 1769–1791.
[23] G. Baril, C. Blanc, N. Pebere, J. Electrochem. Soc. 148 (2001) B489–B496.
[24] G. Baril, C. Blanc, M. Keddam, N. Pebere, J. Electrochem. Soc. 150 (2003) B488–B493.
[25] G. Williams, H.N. McMurray, J. Electrochem. Soc. 155 (2008) C340–C349.
[26] M.J. Franklin, D.C. White, H.S. Isaacs, Corros. Sci. 33 (1992) 251–260.
[27] R.S. Lillard, P.J. Moran, H.S. Isaacs, J. Electrochem. Soc. 139 (1992) 1007–1012.
[28] F. Zou, D. Thierry, H.S. Isaacs, J. Electrochem. Soc. 144 (1997) 1957–1965.
[29] V.M.-W. Huang, V. Vivier, M.E. Orazem, N. Pebere, B. Tribollet, J. Electrochem. Soc. 154 (2007) C81–C88.
[30] V.M.-W. Huang, V. Vivier, I. Frateur, M.E. Orazem, B. Tribollet, J. Electrochem. Soc. 154 (2007) C89–C98.
[31] V.M.-W. Huang, V. Vivier, M.E. Orazem, N. Pebere, B. Tribollet, J. Electrochem. Soc. 154 (2007) C99–C107.
[32] J. Newman, J. Electrochem. Soc. 113 (1966) 501–502.
[33] I. Frateur, V.M.-W. Huang, M.E. Orazem, B. Tribollet, V. Vivier, J. Electrochem. Soc. 154 (2007) C719–C727.
[34] I. Frateur, V.M.-W. Huang, M.E. Orazem, N. Pebere, B. Tribollet, V. Vivier, Electrochim. Acta 53 (2008) 7386–7395.
[35] J.B. Jorcin, M.E. Orazem, N. Pebere, B. Tribollet, Electrochim. Acta 51 (2006) 1473–1479.